Toxicology and Applied Pharmacology 356 (2018) 159–171

Contents lists available at ScienceDirect

Toxicology and Applied Pharmacology

journal homepage: www.elsevier.com/locate/taap

Alantolactone induces apoptosis and improves chemosensitivity of pancreatic cancer cells by impairment of autophagy-lysosome pathway *via* targeting TFEB

Ruizhi He, Xiuhui Shi, Min Zhou, Yan Zhao, Shutao Pan, Chunle Zhao, Xingjun Guo, Min Wang, Xu Li*, Renyi Qin*

Department of Biliary-Pancreatic Surgery, Affiliated Tongji Hospital, Tongji Medical College, Huazhong University of Science and Technology, Wuhan 430030, PR China

ARTICLE INFO

Keywords:
Alantolactone
Autophagy
Lysosome
Apoptosis
Pancreatic cancer

ABSTRACT

The lysosome is emerging as a central regulator of the autophagic process, which plays a critical role in tumor growth and chemoresistance. Alantolactone, which is a natural compound produced by *Inula helenium*, has been shown to induce apoptosis in numerous cancer types. However, the mechanism by which alantolactone regulates apoptosis is still poorly understood. In this work, we observed that alantolactone caused the accumulation of autophagosomes due to impaired autophagic degradation and substantially inhibited the activity and expression of CTSB/CTSD proteins that when depleted caused lysosomal dysfunction. Furthermore, we found that alantolactone inhibited the proliferation of pancreatic cancer cells *in vitro* and *in vivo* and enhanced the chemosensitivity of pancreatic cancer cells to oxaliplatin. In addition, a reduction in TFEB levels was a critical event in the apoptosis and cell death caused by alantolactone. Our data demonstrated that alantolactone, which impaired autophagic degradation, was a pharmacological inhibitor of autophagy in pancreatic cancer cells and markedly enhanced the chemosensitivity of pancreatic cancer cells to oxaliplatin.

1. Introduction

Pancreatic cancer (PC) is a devastating disease due to its malignancy caused by complicated genomic characterization (Torre et al., 2015; Networ, 2017). Despite the continual progress made by surgical advancements, the prognosis of patients remains poor because PC is often resistant to chemotherapies such as gemcitabine and oxaliplatin (Bullock et al., 2017; Middleton et al., 2017). Therefore, new therapeutic options, particularly those that enhance susceptibility to current chemotherapies, are urgently needed.

Macroautophagy (hereafter, autophagy) is a precisely regulated process that is involved in multiple biological activities (Fitzwalter and Thorburn, 2015; Fitzwalter et al., 2018). Autophagy is an evolutionarily conserved catabolic process whereby cellular components are engulfed in double-membraned autophagosomes, which subsequently fuse with the lysosome, and degraded into the cytoplasm (Amaravadi et al., 2016; Kimmelman and White, 2017; Fitzwalter et al., 2018). Although it is well described that autophagy is directed by proteins encoded by autophagy-related genes (ATGs) (Klionsky et al., 2011), there is increasing evidence that lysosomes are emerging as central regulators of the autophagic process and that these regulatory systems are based on the transcription factor (TF) EB, which dominates the CLEAR (coordinated lysosomal expression and regulation) gene network (Medina et al., 2011; Palmieri et al., 2011; Settembre et al., 2011). Basal autophagy is essential to the maintenance of cellular function; thus, autophagy defects are linked to numerous diseases (Choi et al., 2013), including cancer (Amaravadi et al., 2016; Kimmelman and White, 2017), immune and inflammatory diseases (Bhattacharya and Eissa, 2015; Cadwell, 2016), and age-related and degenerative diseases (Rubinsztein et al., 2011). It is well established that suppressing autophagy in genetically engineered mouse models of PC can slow tumor growth and that pharmacological inhibition of autophagy increases cancer cell apoptosis

Abbreviations: PC, pancreatic cancer; Alan, Alantolactone; OxP, oxaliplatin; TFEB, transcription factor EB; CTSB, cathepsin B; CTSD, cathepsin D; ATG5, autophagy-related gene 5; siRNA, small interfering RNA; LC3B, microtubule-associated protein 1 light chain 3β; STX17, syntaxin 17; SNAP29, synaptosome-associated protein 29 kDa; SNAREs, soluble N-ethylmaleimide-sensitive factor attachment protein receptors; CLEAR, coordinated lysosomal expression and regulation; CQ, chloroquine; Baf-A1, bafilomycin A1; LAMP2, lysosomal associated membrane protein 2

* Corresponding author at: Department of Biliary-Pancreatic Surgery, Affiliated Tongji Hospital, Tongji Medical College, Huazhong University of Science and Technology, No.1095 Jie Fang Avenue, Wuhan 430030, PR China.

E-mail addresses: kuai_1985@hotmail.com (X. Li), ryqin@tjh.tjmu.edu.cn (R. Qin).

https://doi.org/10.1016/j.taap.2018.08.003
Received 15 April 2018; Received in revised form 2 August 2018; Accepted 3 August 2018
Available online 04 August 2018

(Rosenfeldt et al., 2013; Yang and Kimmelman, 2014; Li et al., 2016). For this reason, pre-clinical research on autophagy inhibitors may benefit PC treatment.

Alantolactone (Alan), which is a natural product of *Inula helenium*, regulates multiple biological activities, including inhibition of the inflammatory process and induction of apoptosis (Kim et al., 2017; Tang et al., 2018). Previous studies demonstrated that alantolactone induced apoptosis and cell death in numerous cancer types. However, the mechanism by which alantolactone regulates these processes is still unclear (Chun et al., 2015; Wang et al., 2017). Moreover, little research has been conducted on alantolactone in PC to date. In this work, we demonstrated that Alan impaired lysosomal function by inhibiting TFEB, resulting in incomplete autophagy, which led to the apoptosis of PC cells. Importantly, Alan-mediated autophagic obstruction chemosensitized PC cells to oxaliplatin. Our results suggest that the combination of these two agents may serve as a novel strategy for PC therapy.

2. Materials and methods

2.1. Antibodies and reagents

The following antibodies and chemical reagents were purchased: anti-LC3B (3868), anti-SQSTM1 (8025), anti-PARP (9532), anti-caspase-3 (9665), anti-cleaved caspase-3 (9664), and anti-TFEB (37785) were obtained from Cell Signaling Technology (Beverly, MA, USA); anti-GAPDH (60004-1-Ig) and anti-CTSB (12216-1-Ig) were obtained from Proteintech Group (Chicago, IL, USA); anti-CTSD (ab75852) was purchased from Abcam; anti-LAMP2 (sc-18822), anti-Ki67 (sc-15402) antibody were obtained from Santa Cruz Biotechnology (Santa Cruz, CA, USA); alantolactone (SML0415), chloroquine (CQ; C6628), bafilomycin A1 (Baf-A1; B1793), and acridine orange (AO; 01662) were obtained from Sigma-Aldrich (St. Louis, MO, USA); EBSS (24010043) was obtained from ThermoFisher Technology; oxaliplatin (OxP; S1224) was obtained from Selleck (Houston, TX, USA); and LysoTracker Red (L-7528) was purchased from Molecular Probes. *Z*-VAD-FMK was obtained from Millipore (Bedford, MA, USA); and CA-074 methyl ester (HY-100350), aloxistatin (HY-100229) and pepstatin (HY-P0018) were obtained from MCE (Monmouth, NJ, USA).

2.2. Cell lines and culture

Human pancreatic cancer cell lines (MIA PaCa-2 and PANC-1) were purchased from American Type Culture Collection (Manassas, VA, USA). All cells were cultured in Dulbecco's modified Eagle's medium (Gibco) supplemented with 10% fetal bovine serum (FBS) in a 5% CO_2 atmosphere at 37 °C.

2.3. Cell viability assay

Cell viability was assessed with the Cell Counting Kit-8 (CCK-8) assay (Dojindo Molecular Technologies, Kumamoto, Japan) according to the manufacturer's instructions. In brief, cells (3×10^3 per well) were plated in a 96-well plate and treated for 24 h with reagents as indicated by the figures. Water-soluble tetrazolium salt (WST-8) was added to each well and incubated for half an hour at 37 °C with the cells. Absorbance at 450 nm was then measured with a microplate reader (Biotek Instruments, USA). A combination index (CI) was used to study the joint effect of oxaliplatin and alantolactone. The cells were treated with fixed ratios of drug concentrations, and the CI was calculated from the formula using CalcuSyn software.

2.4. Colony formation assay

Cells (1×10^3 per well) were seeded in a 6-well plate. After 24 h, cells were treated with compounds as indicated in the figure legends. After replacing the medium, the cells were cultured for another half a month and then photographed after fixation with 4% paraformaldehyde and 0.1% crystal violet. The colonies (with at least 50 cells/colony) were counted, and statistical tests were used to determine significance.

2.5. Annexin V-FITC/PI apoptosis assay

Cell apoptosis was detected after the indicated treatments by using an annexin V-FITC/PI apoptosis kit (MultiSciences, Hangzhou, China) according to the manufacturer's instructions. After collection following the indicated treatments, the cells were resuspended in 1× binding buffer with annexin V-FITC and PI and incubated in the dark for 15 min at room temperature before being analyzed by flow cytometry on a FACS Calibur flow cytometer (BD Immunocytometry Systems, USA).

2.6. Protein isolation and western blot analysis

For total cellular protein isolation, cells were harvested and lysed on ice in RIPA buffer (Boster Biological Technology, Wuhan, China) with protease inhibitor cocktail for 30 min. After centrifugation at 12,000*g* for 15 min, the supernatant was collected as total cellular protein extract. Protein concentration was measured by the bicinchoninic acid protein assay kit (Beyotime, Haimen, China). An equivalent amount of extracts protein from every sample was resolved on an SDS-PAGE gel and transferred onto a PVDF membrane (Millipore, MA, USA). After incubation with primary antibodies overnight, followed by incubation with specific secondary antibodies coupled to horseradish peroxidase, the blots were then detected with a ChemiDoc XRS System (Bio-Rad Laboratories, USA).

2.7. Acridine orange staining

Acridine orange (AO) is a lysosomotropic weak base that is often used to measure lysosomal function through its accumulation in intracellular acidic vesicles. Cells were stained with AO using the protocol from the manufacturers. Briefly, after treatment with Alan (10 μM, 24 h) or Baf-A1 (100 nM, 24 h), AO (10 μg/ml) was added to cells at 37 °C for 15 min. The cells were washed with phosphate-buffered saline (PBS) three times and then immediately analyzed with an inverted fluorescence microscope (OLYMPUS).

2.8. LysoTracker red staining

Cells were treated with DMSO (6 h), Alan (10 μM, 6 h), or Baf-A1 (100 nM, 6 h) 24 h after they were seeded onto six-well plates. The cells were then collected by trypsin digestion, washed with PBS, and incubated with LysoTracker Red in the dark at room temperature for 30 min. Finally, the fluorescence intensity of the stained cells was immediately assessed by flow cytometry on a FACSCalibur flow cytometer (Becton Dickinson). Data analysis was performed with FlowJo software.

2.9. Cathepsin activity assay

Cathepsin enzymatic activity was detected using fluorometric assay kits for CTSB and CTSD activity (BioVision; K140 and K143) according to the manufacturer's protocol. The cells were collected and lysed in 200 μl of cell lysis buffer after treatment with DMSO (24 h) or Alan (10 μM, 24 h). Then, 50 μl of cell lysate was transferred into 96-well plates, where the reaction buffer and substrate had been previously mixed. The reactions were incubated at 37 °C for 2 h and read in a fluorometer. The enzymatic activity of cathepsins was normalized to the protein concentration of the samples.

2.10. Transmission electron microscopy

After the indicated treatments, cells were fixed in 2.5%

glutaraldehyde in 0.1 M cacodylate buffer at 4 °C overnight and then postfixed with 1% osmium tetroxide in 0.1 M cacodylate buffer for 1 h at 4 °C. After dehydration through a graded series of ethanol, the cells were embedded in spur resin. Serial sections were cut with an ultramicrotome and stained with 4% uranyl acetate and lead citrate. Images were captured by a Hitachi H-7000FA transmission electron microscope.

2.11. Transfection and RNA interference

A lentiviral vector harboring the GFP-LC3B reporter was constructed by GenePharma (Shanghai, China), and transfection was implemented according to the manufacturer's specification. Transfection of the tandem-labeled GFP-mRFP-LC3B and TFEB in the pEnter plasmid was carried out using Lipofectamine 2000 (Invitrogen) according to the manufacturer's instructions. Forty-eight hours after transfection, the cells were incubated with the indicated reagents for further experiments.

The specific small interfering RNA (siRNA, GUGAGAUAUGGUUUG AAUA) targeting ATG5 and the corresponding control were chemically synthesized by Ribobio (Guangzhou, China). The cells were grown in 6-well plates and transfected with 50 nM siRNA using Lipofectamine 2000 (Invitrogen) according to the manufacturer's specifications. Forty-eight hours after transfection, the efficiency of siRNA was monitored by western blot analysis.

2.12. Immunofluorescence and confocal microscopy

For immunofluorescence analysis, cells were seeded on glass coverslips placed in 6-well plates. Following the indicated treatments, cells were fixed with 4% formaldehyde for 30 min and permeabilized with 0.1% Triton X-100 (Sigma-Aldrich) for 10 min. Fixed cells were incubated with primary antibody against TFEB at 4 °C overnight after being blocked with 5% BSA for 30 min at room temperature. The cells were then incubated with Cy3-conjugated secondary antibody for 1 h at 37 °C and counterstained with DAPI (Sigma-Aldrich) for 10 min. Cells were subsequently visualized under a fluorescence microscope.

For confocal microscopy, cells transfected with GFP-LC3B or GFP-mRFP-LC3B were grown on glass coverslips. Following the designated treatments, cells were fixed with 4% formaldehyde for 30 min and photographed using a confocal microscope (Carl Zeiss, Germany, LSM710).

For detection of the fusion of autophagosomes with lysosomes, GFP-LC3B-transfected cells were seeded on glass coverslips. Cells treated with the indicated conditions were fixed with 4% formaldehyde and permeabilized with 0.1% Triton X-100. After blocking with 5% BSA, cells were incubated with antibody against LAMP2 at 4 °C overnight. Cells were then incubated with Cy3-conjugated fluorescent secondary antibody, stained with DAPI, and analyzed with a confocal microscope.

2.13. Autophagic flux measurements

The autophagic flux measured by the LC3B turnover assay was determined by subtracting the densitometric value of the LC3B II amount in untreated samples (LC3B II − CQ) from the corresponding sample treated with chloroquine (LC3B II + CQ) (Aveleira et al., 2015). For each independent experiment, the results are expressed as a percentage of the control.

2.14. Expression profiling in TCGA dataset

TCGA PC mRNA gene expression data were downloaded from UCSC Xena at https://xenabrowser.net/. The gene expression profile was analyzed using the Illumina HiSeq pancan normalized pattern.

2.15. Xenograft experiments

Animal experiments were approved by the Institutional Animal Care and Treatment Committee of Huazhong University of Science and Technology. Female nude BALB/c mice obtained from HFK BioTechnology at 6 to 8 weeks old were subcutaneously injected with PANC-1 cells (2×10^6 per mouse), which were mixed with Matrigel (Becton Dickinson, USA) at a 1:1 ratio. When cells had been successfully implanted, mice were randomized into control and treatment groups ($n = 6$ each). The mice in the control group were intraperitoneally (i.p.) injected with vehicle (10% DMSO, 40% Cremophor/ethanol (3:1), and 50% PBS), while the mice in the alantolactone treatment group received an i.p. injection of alantolactone (3 mg/kg of body weight) according to the indicated frequency. Tumor size and body weight of the mice were measured once a week from the time of implantation. Tumor volume was calculated using the following formula: volume (mm^3) = length × width^2/2. The tumor samples were embedded in paraffin, and subjected to immunohistochemistry staining.

2.16. Statistical analysis

Data are presented as the means ± SD from at least three separate experiments unless otherwise indicated. Significance was evaluated by a two-tailed Student's *t*-test using GraphPad Prism 5 software (GraphPad Software Inc., La Jolla, CA, USA). $P < .05$ was considered statistically significant.

3. Results

3.1. Alan inhibits PC cells growth in vitro and in vivo

To evaluate the effects of Alan on PC cells growth, cell viability assays were carried out in cells treated with increasing concentrations of Alan for 24 and 48 h. Alan partially inhibited the cells viability of MIA PaCa-2 and PANC-1 cells in a dose- and time-dependent manner (Fig. 1B). Next, we performed colony formation assays and revealed that Alan had a similar effect on long-term colony formation by decreasing the number of colonies (Fig. 1C). To verify this finding *in vivo*, we established xenografts of subcutaneously implanted PANC-1 cells. Tumor-bearing mice were randomly divided into control and Alan groups. The mice in the control group were injected with vehicle, whereas the mice in the Alan treatment group received an Alan injection according to the indicated frequency. The mean tumor volume was similar in each group at two weeks post-injection until each group received its corresponding intervention (Fig. 1D). At week 6, treatment with Alan had dramatically inhibited the growth of the xenograft tumors. Meanwhile, weight of mice in each group had no statistically significant difference (Fig. 1D). Immunohistochemistry staining was performed on paraffin-embedded samples of xenograft tumors from the control and Alan groups. The results revealed that Ki67 was lower in the xenograft tumors of the Alan group compared with the control group (Fig. 1E). Collectively, these results demonstrated that Alan inhibited PC cells growth *in vitro* and *in vivo*.

3.2. Alan causes the accumulation of autophagosomes in PC cells

Autophagy is important to support tumor growth in extreme environments (Kimmelman and White, 2017). In recent years, based on the importance of LC3B (microtubule-associated protein 1 light chain 3β) processing for autophagosome formation and function, the detection of LC3B II by immunoblot or fluorescence analysis, together with transmission electron microscopy for assessment of autophagosome formation, has been considered the gold standard technique for monitoring autophagy (Barth et al., 2010). Western blot analysis of endogenous LC3B II expression was carried out to reflect the progression of autophagy. The abundance of LC3B II in MIA PaCa-2 and PANC-1

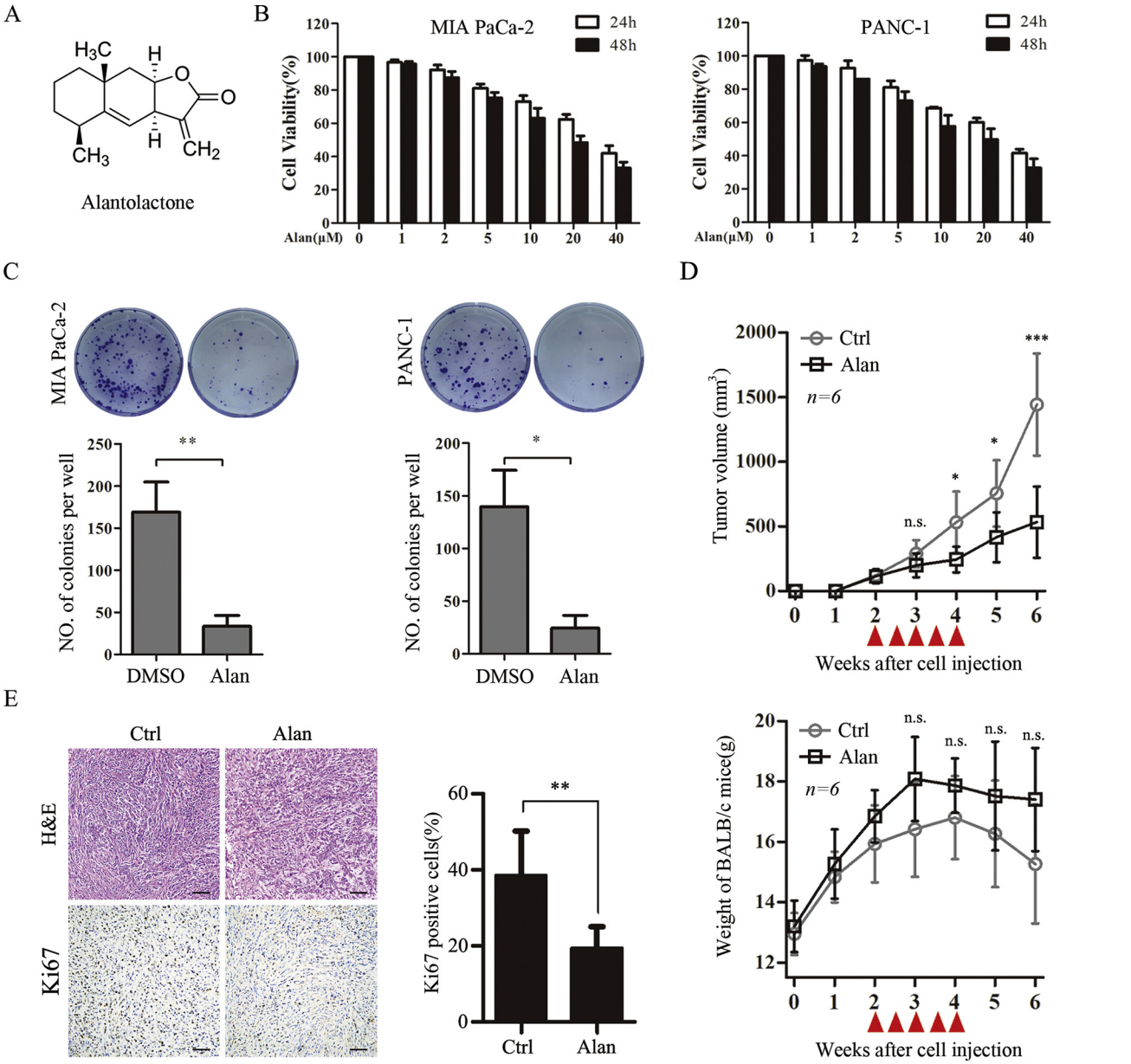

Fig. 1. Alan inhibited PC cells growth *in vitro* and *in vivo*.
(A): Molecular structure of Alan. (B): The indicated cells were treated with Alan at the indicated concentrations and for the indicted duration and then tested for cell viability. (C): MIA PaCa-2 and PANC-1 cells were cultured for 14 days after incubation with Alan (10 μM, 24 h) or DMSO. Representative images are shown (upper panel), and statistical comparisons of the indicated groups were performed (lower panel). Data are represented as the means ± SD ($n = 3$); *, $p < .05$; **, $p < .01$. (D): The tumor volume in each group (upper panel) and body weight (lower panel) of the mice were measured once a week from the time of tumor implantation; the red triangle indicates when the injection was performed. n.s., no significance; *, $p < .05$; ***, $p < .001$. (E): Representative images of immunohistochemistry staining showing H&E and Ki67 in xenograft tumor tissues from the different experimental mouse groups. Specimens were scored and estimated in percentage of positive cells. (For interpretation of the references to colour in this figure legend, the reader is referred to the web version of this article.)

cells was elevated after treatment with Alan in both a dose- and a time-dependent manner (Fig. 2A and Fig. 2B). Treatment of MIA PaCa-2 and PANC-1 cells with Alan at the indicated dose and for the indicated time significantly increased the number of GFP-LC3B puncta compared with that resulting from DMSO treatment, indicating that Alan induced the accumulation of autophagosomes (Fig. 2C). Consistent with these fluorescence data, transmission electron microscopy revealed a 3-fold increase in the number of autophagosomes/autolysosomes in PANC-1 cells that were exposed to Alan at a dose of 10 μM for 24 h compared with that in the group treated with DMSO (Fig. 2D). These findings consistently demonstrate that autophagosomes accumulate when cells are exposed to Alan at the appropriate concentration and for the appropriate duration.

3.3. Alan impairs autophagic degradation, resulting in incomplete autophagy

Autophagosome accumulation in cells may be due to either accelerated autophagosome synthesis or reduced autophagic vacuole maturation and degradation. Chloroquine (CQ), which blocks late-stage autophagy, was used to examine the effect of Alan on autophagosome processes. We evaluated the LC3B II and p62 levels in the absence and presence of CQ and determined autophagic flux by using the LC3B II turnover assay. As expected when lysosome degradation is impaired in

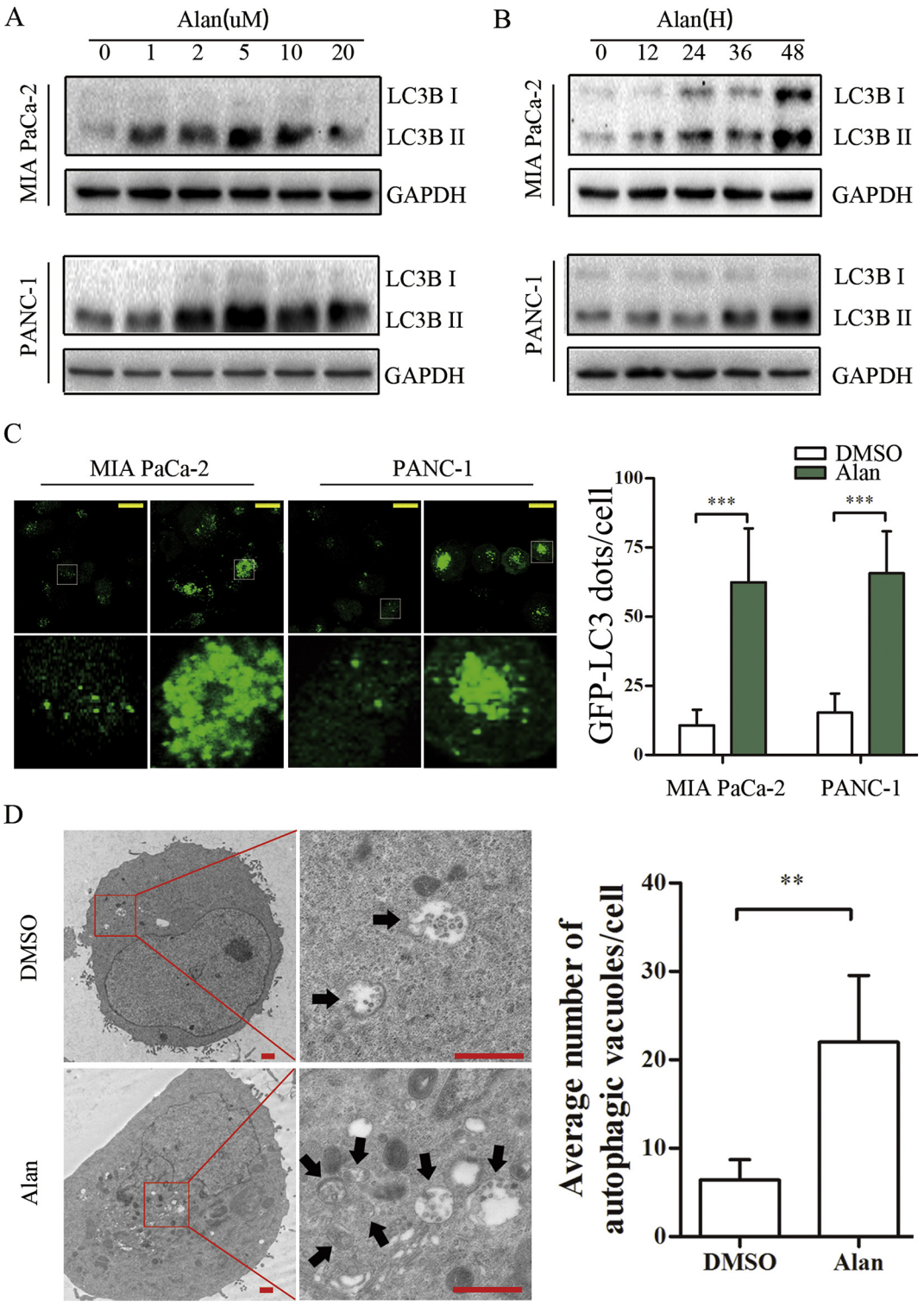

Fig. 2. Alan induced the accumulation of autophagosomes in PC cells.
(A–B): Lysates of MIA PaCa-2 and PANC-1 cells were subjected to western blot analysis of LC3B and GAPDH expression after incubation with either the indicated concentrations of Alan for 24 h or 10 μM Alan for varying periods of time. (C): MIA PaCa-2 and PANC-1 cells transfected with GFP-LC3B were treated with 10 μM Alan for 24 h, and representative confocal images are shown in the left panel; the number of LC3 dots is quantified in the right panel, and at least 30 cells were included in each group. Data are presented as the means ± SD from 3 independent experiments (***, $p < .001$). Scale bar: 20 μm. (D): PANC-1 cells treated with Alan (10 μM) or DMSO for 24 h were imaged by transmission electron microscopy to detect characteristic autophagosomes/autolysosomes. Representative images and their magnified view are shown in the left panel. The right panel is the quantification of the number of autophagic vacuoles from at least 15 areas. Arrowhead: autophagic vacuoles; Scale bar: 1 μm.

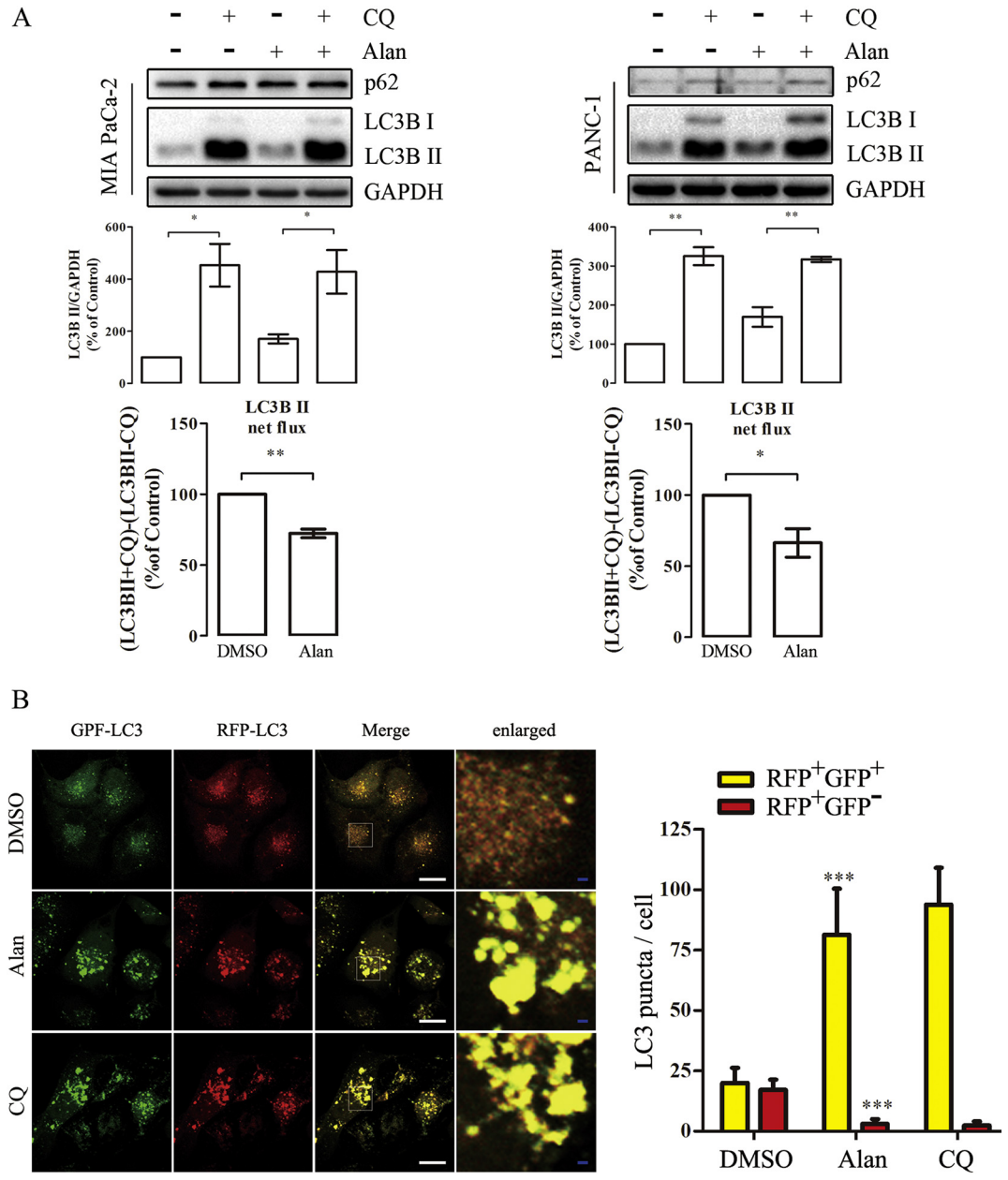

Fig. 3. Alan suppressed the autophagic flux in PC cells.
(A): MIA PaCa-2 and PANC-1 cells were exposed to Alan (10 μM, 24 h) in the absence or presence of CQ (10 μM, 16 h). Cell lysates were analyzed for protein levels of LC3 and p62 by western blot analysis. Upper panels: representative bands; middle panels: quantitative analysis of relative protein levels from triplicate independent experiments; lower panels: LC3B II net flux as determined by subtracting the densitometric value of LC3B II in samples not treated with CQ (LC3B II − CQ) from the corresponding sample treated with chloroquine (LC3B-II + CQ); *, $p < .05$; **, $p < .01$. (B): PANC-1 cells were treated with Alan (10 μM, 24 h) and CQ (10 μM, 16 h) after transfection with GFP-mRFP-LC3B and then photographed using confocal microscopy. Representative images of autophagosome (yellow puncta) and autolysosome (red puncta) formation are presented in the left panel. Scale bar: 20 μm (white) and 2 μm (blue). The numbers of yellow (RFP^+GFP^+) puncta and red (RFP^+GFP^-) puncta are shown in the right panel. ***, $p < .001$ compared with the control. (For interpretation of the references to colour in this figure legend, the reader is referred to the web version of this article.)

the presence of CQ, LC3B II and p62 levels accumulated in treated cells rather than in those incubated in the absence of CQ based on western blot analysis (Fig. 3A). Autophagic flux represents the amount of LC3B II delivered into the lysosome and is determined by comparing the LC3B II amounts in samples in the presence and absence of CQ (Aveleira et al., 2015; Klionsky et al., 2016). We demonstrated that Alan decreased the LC3B II net flux in PANC-1 cells (Fig. 3A). A tandem-labeled GFP-mRFP-LC3 reporter was also used to measure autophagic flux. In this system, the GFP-mRFP-LC3 reporter localizes as yellow puncta in autophagosomes and red-only puncta in autolysosomes because the GFP fluorescence of this reporter decays in the acidic lysosomal environment, whereas mRFP is more resistant to low pH (Li et al., 2016). Treatment of cells with either Alan or CQ increased the amount of GFP-mRFP-LC3 yellow puncta compared with that resulting from DMSO treatment, and conversely, the number of red-only puncta was decreased (Fig. 3B). Taken together, these data indicate that Alan is a potent autophagic inhibitor that accumulates in autophagosomes due to impaired autophagic degradation.

3.4. Alan causes lysosomal dysfunction in PC cells

Impaired autophagic degradation is closely related to the

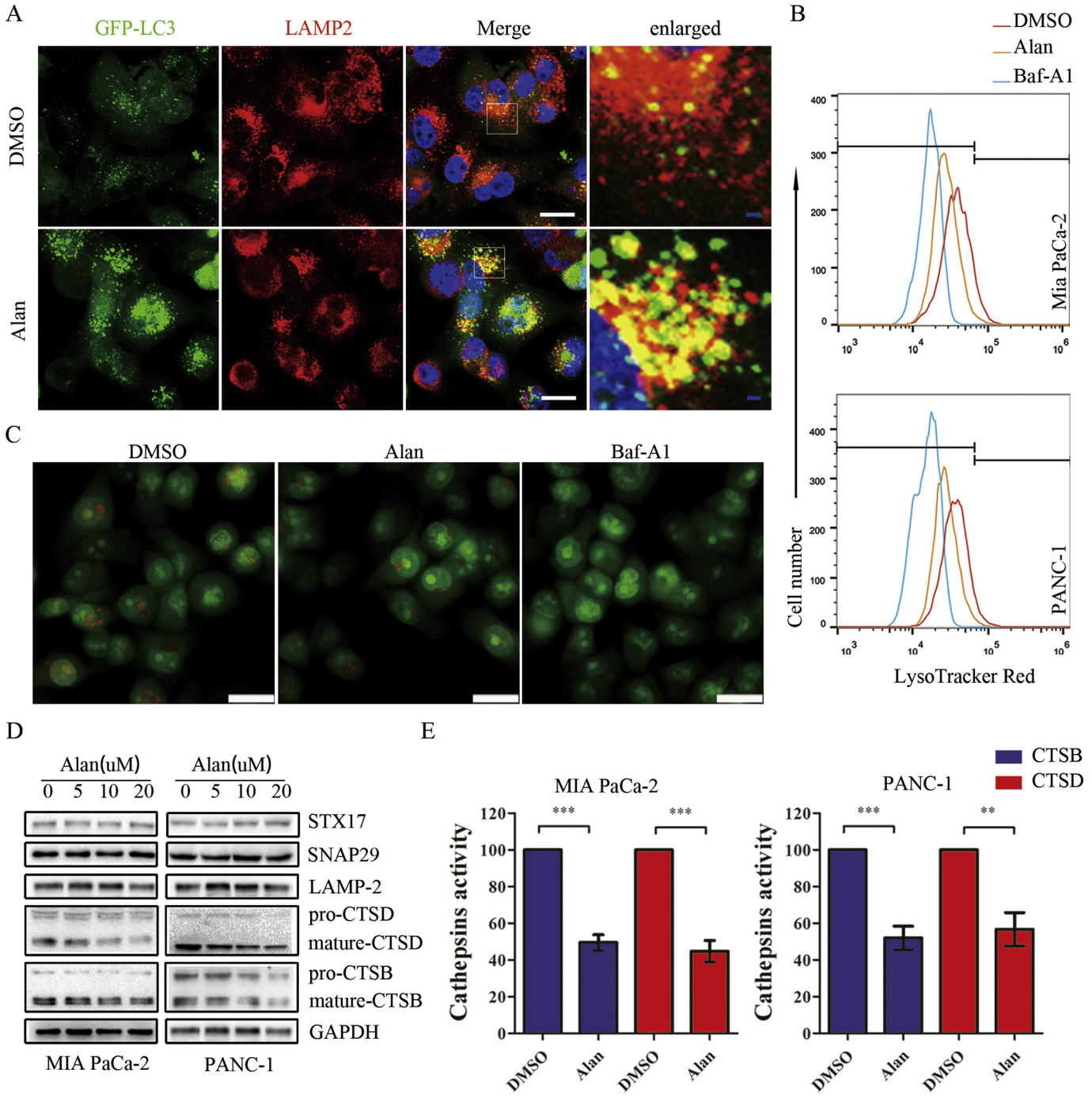

Fig. 4. Alan inhibited lysosomal hydrolases, resulting in lysosomal dysfunction, but did not affect the fusion of autophagosomes and lysosomes.
(A): GFP-LC3B-transfected PANC-1 cells were incubated with Alan (20 μM) for 24 h and then immunostained for LAMP2, followed by DAPI staining of nuclei. Representative confocal images are shown, and the panels on the right are higher magnification images. Scale bar: 20 μm (white) and 2 μm (blue). (B): FACS analysis of LysoTracker Red after MIA PaCa-2 and PANC-1 cells were treated with Alan (10 μM) and Baf-A1 (100 nM) for 24 h. (C): PANC-1 cells were stained with 10 μg/ml acridine orange at 37 °C for 15 min after incubation with Alan and Baf-A1 (negative control) for 24 h. Scale bar: 25 μm. (D): Western blot analysis of autolysosome -associated protein expression after treatment with Alan for 24 h at the indicated concentrations. (E): Enzymatic activity of CTSB and CTSD in Alan-treated PC cells. After treatment with Alan (10 μM, 24 h), enzymatic activity was analyzed using fluorogenic kits. Data are presented as the means ± SD from 3 independent experiments; **, $p < .01$; ***, $p < .001$. (For interpretation of the references to colour in this figure legend, the reader is referred to the web version of this article.)

immaturity of autolysosomes and is caused by either defective fusion between autophagosomes and lysosomes or lysosomal dysfunction (Song et al., 2017). To determine whether Alan affects the fusion of autophagosomes and lysosomes, confocal microscopy was used to determine the colocalization between GFP-LC3B and LAMP2 (lysosomal associated membrane protein 2, a marker of lysosomes). PANC-1 cells treated with Alan exhibited colocalization between LC3B (green puncta) and LAMP2 (red puncta) that was similar to that in cells treated with DMSO (Fig. 4A). Fusion of autophagosomes with lysosomes is mediated by soluble N-ethylmaleimide-sensitive factor attachment protein receptors (SNAREs), which are composed of STX17 (syntaxin 17) and SNAP29 (synaptosome-associated protein 29 kDa) (Itakura et al., 2012). Consistently, the abundance of STX17 and SNAP29 had not changed upon Alan treatment (Fig. 4D). These data indicated that

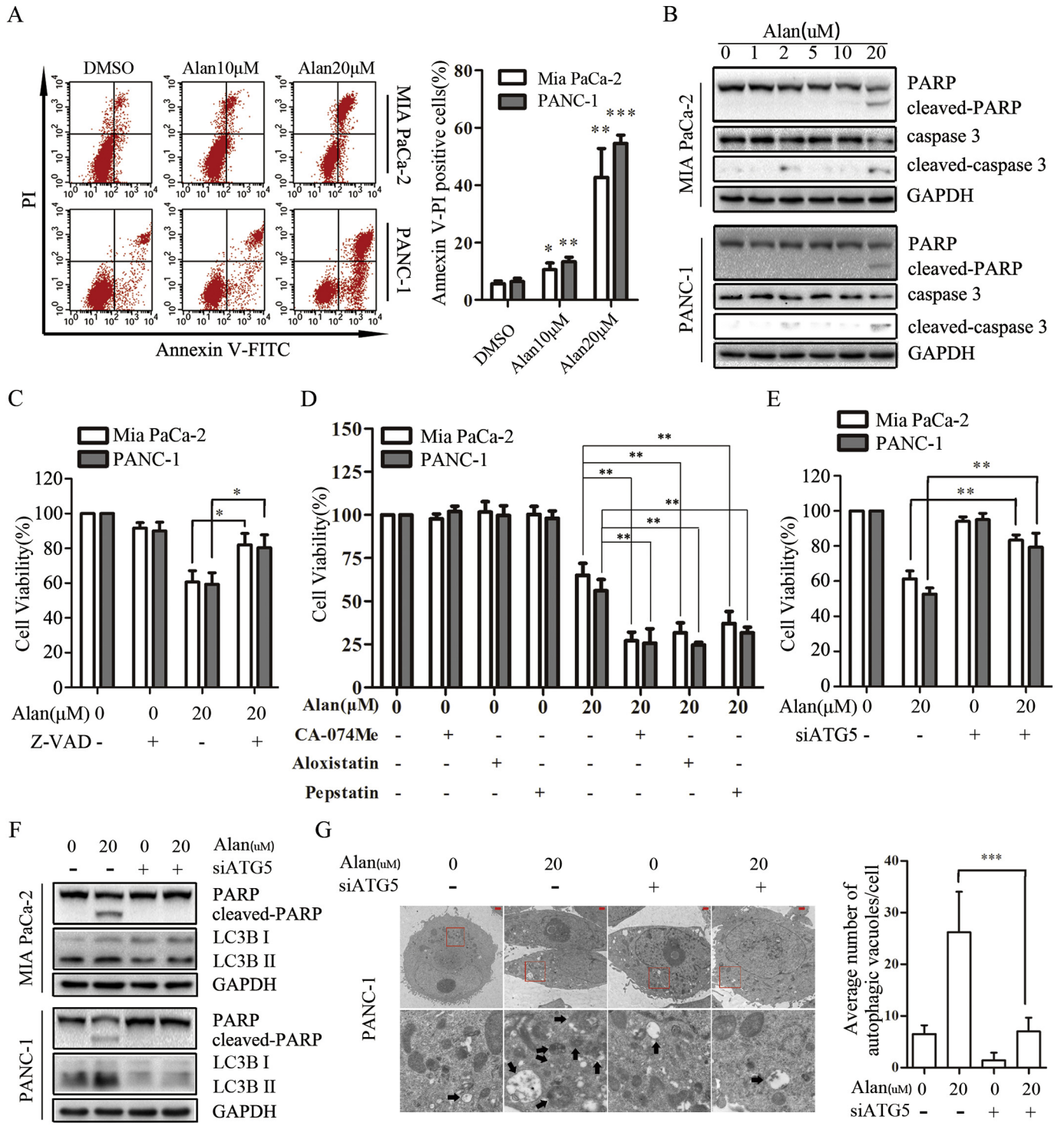

Fig. 5. Alan induced cytotoxic autophagosome-dependent apoptosis and cell death.
(A): Results of the FACS analysis of apoptosis after the treatment of PC cells with Alan at the indicated concentrations for 24 h are shown in the left panel. Apoptotic cell results are shown in the right panel, and the data are shown as the means ± SD. (B): Western blot analysis of PARP, cleaved PARP, caspase-3, and cleaved caspase-3 levels was performed on lysates from MIA PaCa-2 and PANC-1 cells treated with Alan at the indicated concentration for 24 h. (C-D): MIA PaCa-2 and PANC-1 cells were pre-treatedwith either *Z*-VAD (50 μM) or inhibitors of lysosomal hydrolases (5 μM CA-074Me, 5 μM aloxistatin, 5 μM pepstatin) for 1 h, followed by a 24-h treatment with Alan (20 μM), and cell viability was subsequently assessed. Data are represented as the means ± SD ($n = 3$); *, $p < .05$; **, $p < .01$. (*E*-G): MIA PaCa-2 and PANC-1 cells were transfected with siRNA against ATG5 and then subjected to cell viability assays, western blot analysis and transmission electron microscopy as indicated. Arrowhead: autophagic vacuoles; Scale bar: 1 μm. Data are presented as the means ± SD (n = 3); **, $p < .01$.

Alan did not affect autophagosome-lysosome fusion. Thus, subsequent experiments were performed to examine lysosomal function. Two specific probes for live-cell lysosome labeling were used to assess lysosomal function. First, LysoTracker Red staining was analyzed by flow cytometry. LysoTracker Red fluorescence intensity was lower in Alan-treated cells compared with control cells, but higher in Alan-treated cells compared with in cells treated with Baf-A1, which significantly reduced fluorescence intensity (Fig. 4B), as Baf-A1 disrupts the normal

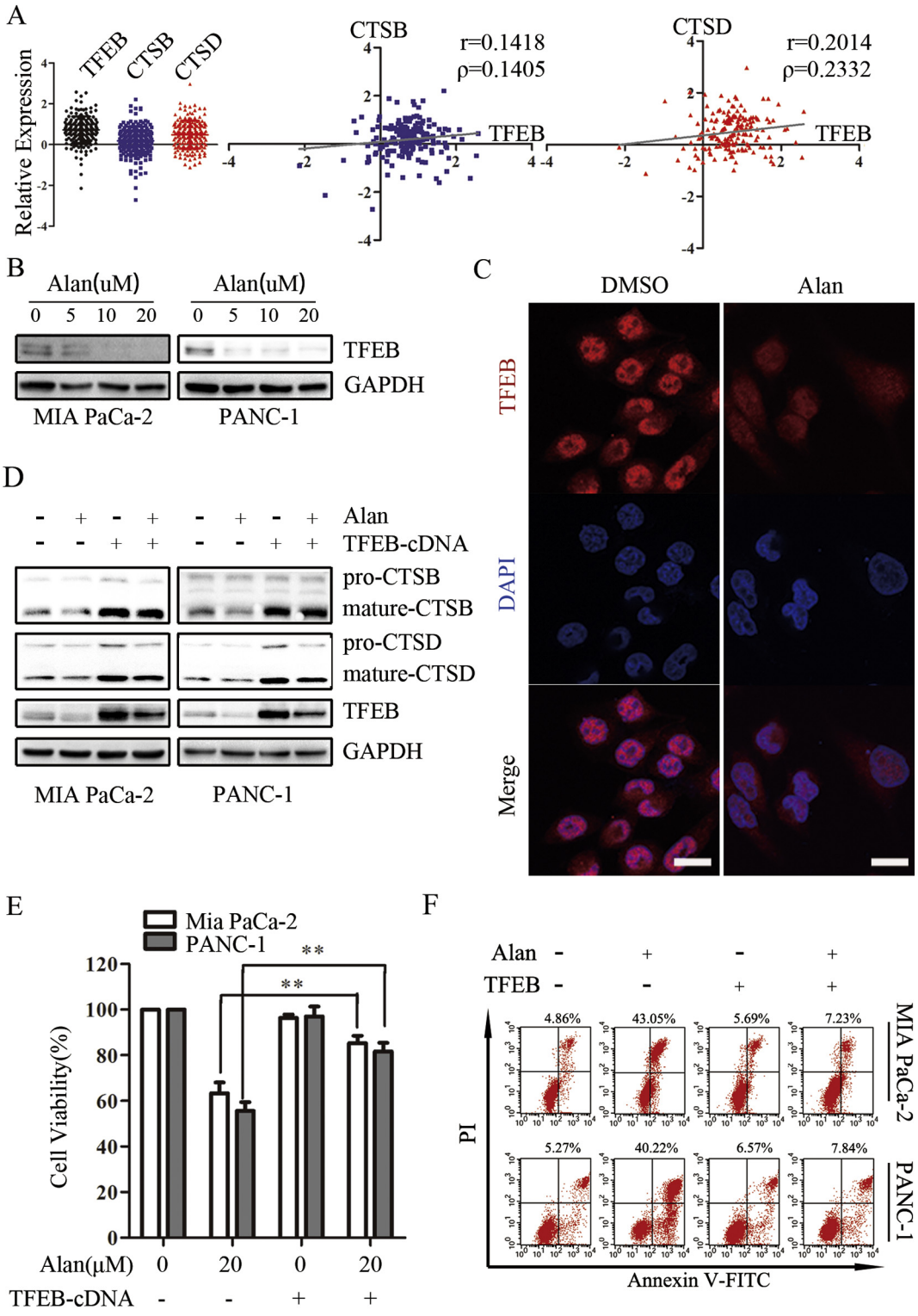

Fig. 6. Identification of TFEB as a critical regulatory factor in Alan-induced apoptosis of PC cells.
(A): Analysis of expression correlation based on a TCGA dataset of 196 pancreatic cancer patients. (B): Protein lysates from cells treated with the indicated concentration of Alan for 24 h were subjected to western blot analysis as indicated. (C): After incubation with Alan (10 μM) for 24 h, PANC-1 cells were subjected to immunofluorescence as indicated. Scale bar: 20 μm. (D-F): MIA PaCa-2 and PANC-1 cells were pre-transfected with TFEB *via* the pEnter plasmid, followed by a 24-h treatment with Alan (20 μM), and they were subsequently subjected to Western blot, cell viability and annexin V-FITC/PI apoptosis assays as indicated. Results of annexin V-PI positive cells are shown as indicated.

function of the lysosome by neutralizing lysosomal pH (Li et al., 2016). Second, AO staining exhibits green fluorescence in the cytoplasm but red fluorescence when it enters acidic vesicles (Boya and Kroemer, 2008), Treatment of PANC-1 cells with Alan resulted in reduced amounts of red fluorescence following AO staining compared with that in cells treated with DMSO (Fig. 4C). Thus, the results indicate Alan caused lysosomal alkalinization in PC cells. Moreover, lysosomal degradation depends on the amount and activity of hydrolases, and

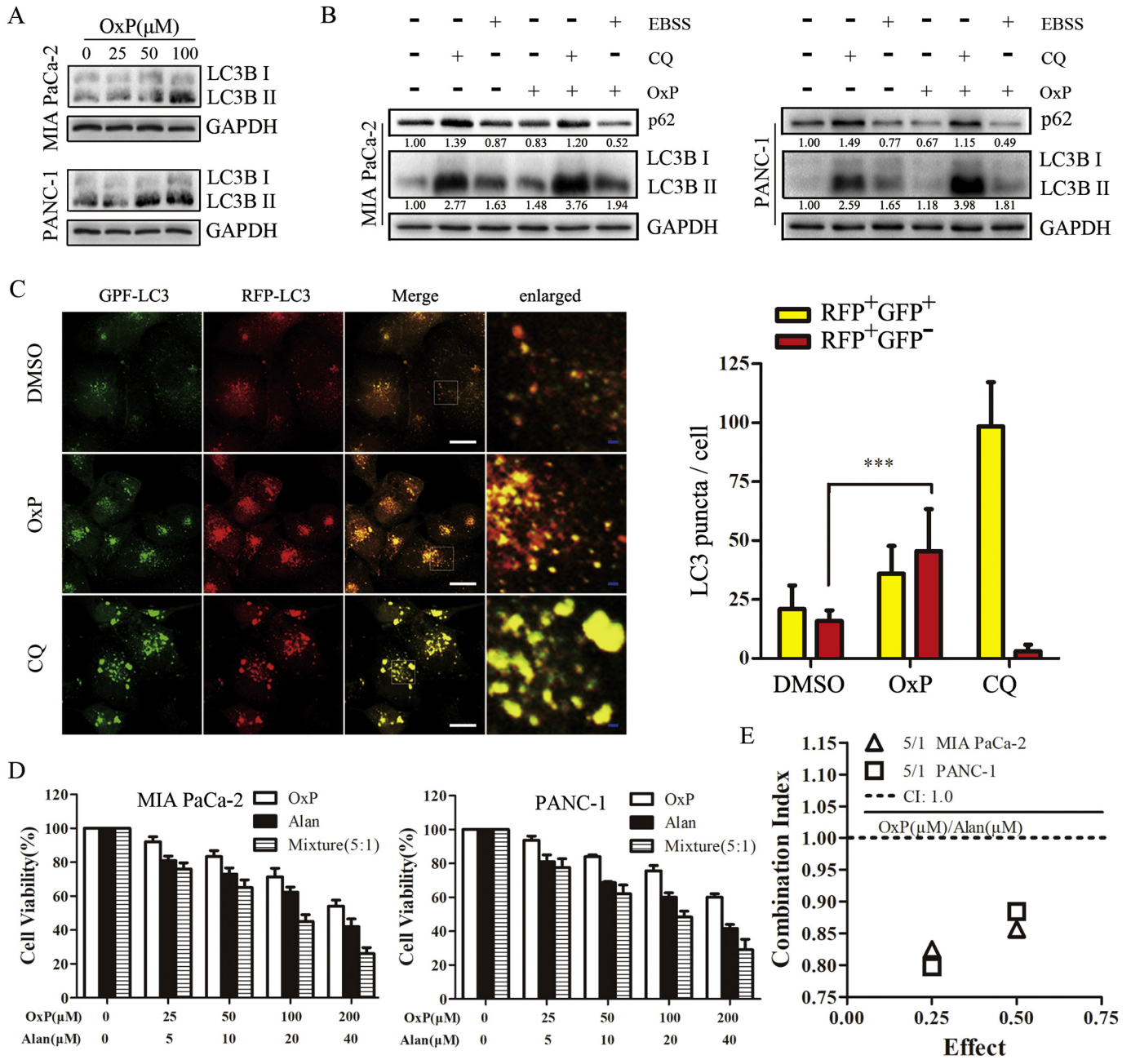

Fig. 7. Alan enhances the chemosensitivity of pancreatic cancer cells to oxaliplatin.
(A): Lysates of MIA PaCa-2 and PANC-1 cells were subjected to western blot analysis for LC3B and GAPDH expression after the cells were incubated with the indicated concentrations of oxaliplatin for 24 h. (B): MIA PaCa-2 and PANC-1 cells were exposed to oxaliplatin (25 μM, 24 h) in the absence or presence of either CQ (10 μM, 16 h) or EBSS (2 h). Cell lysates were analyzed for protein levels of LC3 and p62 by western blot analysis. Results of relative quantitative analysis of p62 are shown as indicated. (C): PANC-1 cells were treated with oxaliplatin (25 μM, 24 h) and CQ (10 μM, 16 h) after transfection with GFP-mRFP-LC3B and then photographed using confocal microscopy. Representative images of autophagosome (yellow puncta) and autolysosome (red puncta) formation are shown in the left panel. Scale bar: 20 μm (white) and 2 μm (blue). Quantification of the number of yellow (RFP + GFP+) puncta and red (RFP + GFP-) puncta is shown in the right panel. ***, $p < .001$ compared with the control. (D): MIA PaCa-2 and PANC-1 cells were treated with oxaliplatin, Alan or the two in combination at a fixed ratio (5:1) at the indicated concentrations for 24 h, and cell viability assays were then performed. (E): The combination index (CI) values for oxaliplatin and Alan in MIA PaCa-2 and PANC-1 cells were determined using CalcuSyn software. Synergy was defined as CI values < 1.0. (For interpretation of the references to colour in this figure legend, the reader is referred to the web version of this article.)

cathepsins are the most studied lysosomal hydrolases that participate in autophagic or lysosomal degradation (Settembre et al., 2013). We then investigated whether Alan affects the expression and enzymatic activity of CTSB (cathepsin B) and CTSD (cathepsin D). Under the same Alan treatment conditions, reduced expression of CTSB and CTSD was observed at the protein level and primarily involved the mature forms of the proteins (Fig. 4D). Consistently, treatment of MIA PaCa-2 and PANC-1 cells with Alan decreased the activity of proteases compared with that in those treated with DMSO (Fig. 4E). Taken together, these data verified that Alan caused lysosomal dysfunction due to lysosomal alkalinization and inhibition of the activity and expression of CTSB/CTSD simultaneous. Moreover, impaired autophagic degradation caused by Alan is attributed to lysosomal dysfunction rather than impaired fusion between autophagosomes and lysosomes.

3.5. Alan-induced incomplete autophagy promotes apoptosis and cell death

Increasing evidence demonstrates that autophagy can protect cancer cells against apoptosis (Fitzwalter and Thorburn, 2015). Thus, it was imperative to determine whether the incomplete autophagy induced by Alan was associated with apoptosis. We used annexin V/PI to assess whether Alan induced apoptosis. PC cells treated with Alan underwent apoptosis within 24 h of treatment in a dose-dependent manner (Fig. 5A). Cleaved PARP, which is the product of PARP after cleavage by cleaved caspase-3, is considered a marker of apoptosis (Agarwal et al., 2009). Consistently, treatment of PC cells with Alan decreased the expression of PARP and caspase-3 in a dose-dependent manner while increasing the level of cleaved PARP and cleaved caspase-3 (Fig. 5B). To assess whether this caspase activity was dependent on Alan-induced apoptosis, the cell-permeable pan-caspase inhibitor *Z*-VAD-FMK was used. Cell death caused by Alan was notably reduced in cells pre-treated with Z-VAD-FMK (Fig. 5C). Lysosomal dysfunction can potentially induce lysosomal membrane permeabilization (LMP) due to the translocation of abundant hydrolases from the lysosome to the cytoplasm (Song et al., 2017). To explore whether LMP was involved in Alan-induced apoptosis, specific inhibitors of hydrolases were used. Pre-incubation of MIA PaCa-2 and PANC-1 cells with CA-074Me (CTSB inhibitor), aloxistatin (cysteine protease inhibitor), or pepstatin (CTSD inhibitor) further increased the growth inhibition induced by Alan, while these agents alone had no effect on cell viability (Fig. 5D). The level of cleaved PARP also increased in cells treated with both Alan and aloxistatin (Fig. S1A). In contrast, knockdown of the ATG5 (autophagy related 5) gene in PC cells attenuated the inhibition of proliferation by Alan (Fig. 5E and Fig. S1B). Consistent with this finding, the PARP cleavage induced by Alan was rescued by silencing the expression of ATG5 (Fig. 5F). Furthermore, knockdown of ATG5 attenuated Alan-caused accumulation of autophagosomes (Fig. 5F and G). Thus, we conclude that Alan induced cytotoxic autophagic cell death in PC cells and that decreased activity of lysosomal hydrolases rather than LMP was responsible for the apoptosis induced by Alan.

3.6. Reduced levels of TFEB is a critical event in the apoptosis induced by Alan

The transcription factor EB (TFEB), a master regulator of lysosomal biogenesis and function, regulates the CLEAR gene network, which includes the CTSB and CTSD genes (Palmieri et al., 2011). To assess whether there is a correlation between the expression of TFEB and that of CTSB or CTSD, a TCGA dataset including 196 PC patients with mRNA expression of TFEB/CTSB/CTSD was analyzed (Fig. 6A) (TCGA, 2018). It suggests that the expression of TFEB was associated with CTSB/CTSD expression (Fig. 6A). We next demonstrated that the abundance of TFEB decreased in a dose-dependent manner after treatment of PC cells with Alan (Fig. 6B). Treatment of PANC-1 cells with Alan decreased the fluorescence intensity of TFEB compared with that of cells treated with DMSO, particularly in the nucleus (Fig. 6C). Moreover, expression of TFEB *via* the pEnter plasmid was used to ascertain whether TFEB plays a significant role in Alan-induced lysosomal dysfunction. Pre-transfection with TFEB upregulated the expression of CTSB and CTSD in MIA PaCa-2 and PANC-1 cells, and the expression of TFEB not only strikingly rescued the reduction of CTSB and CTSD expression caused by Alan (Fig. 6D) but also partially abrogated Alan-induced apoptosis (Fig. 6E) and cell death (Fig. 6F). These results provided evidence that TFEB is a key factor regulating lysosomal function and that a reduction in TFEB is a critical event in the apoptosis and cell death caused by Alan.

3.7. Alan enhances the chemosensitivity of PC cells to oxaliplatin

It is well established that autophagy promotes therapeutic resistance by protecting cells from apoptosis during the stress of chemotherapy (Rebecca and Amaravadi, 2016). Thus, it is important to determine the level of autophagy in PC cells during treatment with chemotherapeutics. The abundance of LC3B II in MIA PaCa-2 and PANC-1 cells increased in a dose-dependent manner when cells were treated with gradually increasing concentrations of oxaliplatin (Fig. 7A). To determine the actual role of oxaliplatin, its effects were evaluated by western blot analysis in the presence of CQ and EBSS. Co-incubation of cells with oxaliplatin and CQ caused a significant increase in LC3B II compared with incubation with CQ alone (Fig. 7B), and co-administration of oxaliplatin and EBSS markedly decreased the expression level of p62 compared with that in cells treated with EBSS alone. Consistent with these results, treatment of PANC-1 with oxaliplatin not only increased the amount of total LC3 puncta but also increased the red puncta mainly compared with that in cells treated with DMSO, while CQ significantly increased the presence of GFP-mRFP-LC3 puncta (Fig. 7C). This finding revealed that autophagic flux was simulated during the exposure of PC cells to oxaliplatin. We next investigated whether Alan sensitized PC cells to oxaliplatin-induced cell death by cell viability assays. Combination treatment of MIA PaCa-2 and PANC-1 cells with Alan and oxaliplatin elevated the growth inhibitory ratio compared with either agent alone (Fig. 7D). To ascertain whether the effect of the combination of these agents was additive or synergistic, CI values were calculated using the CalcuSyn software. CI values quantify the interaction of mutually exclusive agents that have independent modes of action, and CI = 1 indicates an additive effect, CI < 1 indicates synergy, and CI > 1 suggests antagonism (Crescenzi et al., 2006). When PC cells were treated with oxaliplatin and Alan at a fixed concentration ratio for 24 h, CI values of 0.825 and 0.798 and CI values of 0.856 and 0.884 were calculated for a 25% inhibitory effect and a 50% inhibitory effect in MIA PaCa-2 and PANC-1 cells, respectively, which revealed that oxaliplatin and Alan acted in a synergistic manner (Fig. 7E). Taken together, these data suggest that induced autophagic flux functions to promote PC cells survival during oxaliplatin treatment and Alan enhances the chemosensitivity of PC cells to oxaliplatin.

4. Discussion

Here, we report that Alan is a pharmacological inhibitor of autophagy in PC cells by inducing incomplete autophagy due to impaired autophagic degradation. Autophagy is a dynamic and continuous process involving the formation of autophagosomes (early stage) and lysosomal degradation after fusing (late stage) (Klionsky et al., 2016). In our study, we found that Alan caused the accumulation of autophagosomes in PC cells. However, autophagosome accumulation in cells may be due to either accelerated autophagosome synthesis or reduced autophagic vacuole maturation and degradation. We therefore used autophagic flux assays to determine that Alan impaired autophagy during the late stage. The impairment of autolysosomes depends on either the defective fusion between autophagosomes and lysosomes or lysosomal dysfunction (Song et al., 2017). Functional lysosomes have the unique feature of a highly acidic pH, which depends on both the activity or expression of lysosomal hydrolases and the integrity of the lysosomal membrane (Zhou et al., 2013). Surprisingly, Alan substantially caused lysosomal dysfunction due to lysosomal alkalinization and inhibition of the activity and expression of CTSB/CTSD simultaneous. Furthermore, we identified that a reduction in TFEB is a critical event in the apoptosis and cell death induced by Alan. TFEB regulates lysosomal biogenesis and function (Settembre and Ballabio, 2011; Settembre et al., 2011). We observed that TFEB could partially abrogate Alan-induced apoptosis and cell death. Therefore, the ability of Alan to impair autophagy at the late stage mainly depends on the strong association between lysosomal biogenesis and autophagy.

Autophagy has complicated effects on cancer; although autophagy has been shown to have a critical role in fighting the transformation of normal cells, it plays a role in promoting proliferation and invasion in multiple types of pre-existing cancers (White, 2015; Kimmelman and

White, 2017). For this reason, numerous studies are being conducted on the inhibition of autophagy for cancer therapies, including ongoing clinical trials (Levy et al., 2017). We thus found that Alan caused PC cells death *in vitro* and inhibited PC cells growth *in vivo* and induced caspase-dependent apoptosis. Interestingly, knockdown of ATG5 abrogated the ability of Alan to cause PC cells death, and attenuated Alan-caused accumulation of autophagosomes. Depletion of ATG5, an essential autophagy gene, inhibited autophagosome formation during early autophagy (Kimmelman and White, 2017). These strongly suggest that Alan-induced apoptosis was dependent on cytotoxic autophagosomes. Additionally, lysosomal membrane stability is necessary to prevent the acidic hydrolases from accessing the cytosol, which would result in cell death (Boya and Kroemer, 2008). In our work, we found that an LMP inhibitor further increased the growth suppression of PC cells induced by Alan, indicating that decreased activity of lysosomal hydrolases, rather than LMP, was responsible for Alan-induced apoptosis.

Like many other tumor types, PC exhibits elevated basal levels of autophagy compared with normal tissue (Yang et al., 2011; Kimmelman and White, 2017). Previous studies demonstrated that autophagy promotes therapeutic resistance during chemotherapy in PC (Rebecca and Amaravadi, 2016; Fitzwalter et al., 2018). Here, we determined that oxaliplatin induced autophagy while killing cancer cells and further confirmed that Alan-induced incomplete autophagy improves the anticancer therapeutic effect of oxaliplatin. Therefore, it is possible to leverage this protective autophagy to increase the efficacy of chemotherapeutics (Ding et al., 2011; Rebecca and Amaravadi, 2016; Fitzwalter et al., 2018).

5. Conclusions

In summary, here, we identified Alan as a pharmacological inhibitor of autophagy in PC cells that induces incomplete autophagy due to a reduced expression level of TFEB, which causes lysosomal dysfunction, leading to impaired autophagic degradation. Moreover, Alan-induced incomplete autophagy markedly enhanced the chemosensitivity of PC cells to oxaliplatin. These findings will help facilitate the development of combination therapies for inhibiting autophagy. Moreover, the combination therapy of oxaliplatin and Alan could become a novel approach for PC treatment.

Supplementary data to this article can be found online at https://doi.org/10.1016/j.taap.2018.08.003.

Ethics approval

All animal experiments complied with the ARRIVE guidelines and were carried out in accordance with the National Institutes of Health guide for the care and use of Laboratory animals and the guidelines of the Huazhong University of Science and Technology.

Consent for publication

We have obtained consents to publish this paper from all the participants of this study.

Availability of data and material

All data generated or analyzed during this study are included in this published article.

Competing interests

The authors declare that they have no competing interests.

Authors' contributions

Xu Li and Renyi Qin designed the study; Ruizhi He performed the experiments; Xiuhui Shi, Min Zhou and Yan Zhao collected the data; Shutao Pan and Chunle Zhao analyzed the data; Xingjun Guo and Min Wang guided analysis of the data; and all the authors read and approved the final manuscript.

Acknowledgements

This study was supported by the National Natural Science Foundation of China (No. 81502633 to Xu Li, No. 81773160 to Min Wang, No. 81772950 to Renyi Qin).

References

Agarwal, A., Mahfouz, R.Z., Sharma, R.K., Sarkar, O., Mangrola, D., Mathur, P.P., 2009. Potential biological role of poly (ADP-ribose) polymerase (PARP) in male gametes. Reprod. Biol. Endocrinol. 7, 143.
Amaravadi, R., Kimmelman, A.C., White, E., 2016. Recent insights into the function of autophagy in cancer. Genes Dev. 30, 1913–1930.
Aveleira, C.A., Botelho, M., Carmo-Silva, S., Pascoal, J.F., 2015. Neuropeptide Y Stimulates Autophagy in Hypothalamic Neurons. vol. 112. pp. E1642–E1651.
Barth, S., Glick, D., Macleod, K.F., 2010. Autophagy: assays and artifacts. J. Pathol. 221, 117–124.
Bhattacharya, A., Eissa, N.T., 2015. Autophagy as a stress response pathway in the immune system. Int. Rev. Immunol. 34, 382–402.
Boya, P., Kroemer, G., 2008. Lysosomal membrane permeabilization in cell death. Oncogene 27, 6434–6451.
Bullock, A., Stuart, K., Jacobus, S., Abrams, T., Wadlow, R., Goldstein, M., Miksad, R., 2017. Capecitabine and oxaliplatin as first and second line treatment for locally advanced and metastatic pancreatic ductal adenocarcinoma. J. Gastrointest. Oncol. 8, 945–952.
Cadwell, K., 2016. Crosstalk between autophagy and inflammatory signalling pathways: balancing defence and homeostasis. Nat. Rev. Immunol. 16, 661–675.
Choi, A.M., Ryter, S.W., Levine, B., 2013. Autophagy in human health and disease. N. Engl. J. Med. 368, 651–662.
Chun, J., Li, R.J., Cheng, M.S., Kim, Y.S., 2015. Alantolactone selectively suppresses STAT3 activation and exhibits potent anticancer activity in MDA-MB-231 cells. Cancer Lett. 357, 393–403.
Crescenzi, E., Chiaviello, A., Canti, G., Reddi, E., Veneziani, B.M., Palumbo, G., 2006. Low doses of cisplatin or gemcitabine plus Photofrin/photodynamic therapy: Disjointed cell cycle phase-related activity accounts for synergistic outcome in metastatic non-small cell lung cancer cells (H1299). Mol. Cancer Ther. 5, 776–785.
Ding, Z.B., Hui, B., Shi, Y.H., Zhou, J., Peng, Y.F., Gu, C.Y., Yang, H., Shi, G.M., Ke, A.W., Wang, X.Y., Song, K., Dai, Z., Shen, Y.H., Fan, J., 2011. Autophagy activation in hepatocellular carcinoma contributes to the tolerance of oxaliplatin via reactive oxygen species modulation. Clin. Cancer Res. 17, 6229–6238.
Fitzwalter, B.E., Thorburn, A., 2015. Recent insights into cell death and autophagy. FEBS J. 282, 4279–4288.
Fitzwalter, B.E., Towers, C.G., Sullivan, K.D., Andrysik, Z., Hoh, M., Ludwig, M., O'Prey, J., Ryan, K.M., Espinosa, J.M., Morgan, M.J., Thorburn, A., 2018. Autophagy inhibition mediates apoptosis sensitization in cancer therapy by relieving FOXO3a turnover. Dev. Cell 44, 555–565 (e553).
Itakura, E., Kishi-Itakura, C., Mizushima, N., 2012. The hairpin-type tail-anchored SNARE syntaxin 17 targets to autophagosomes for fusion with endosomes/lysosomes. Cell 151, 1256–1269.
Kim, M., Song, K., Kim, Y.S., 2017. Alantolactone improves palmitate-induced glucose intolerance and inflammation in both lean and obese states in vitro: adipocyte and adipocyte-macrophage co-culture system. Int. Immunopharmacol. 49, 187–194.
Kimmelman, A.C., White, E., 2017. Autophagy and tumor metabolism. Cell Metab. 25, 1037–1043.
Klionsky, D.J., Baehrecke, E.H., Brumell, J.H., Chu, C.T., Codogno, P., Cuervo, A.M., Debnath, J., Deretic, V., Elazar, Z., Eskelinen, E.L., Finkbeiner, S., Fueyo-Margareto, J., Gewirtz, D., Jaattela, M., Kroemer, G., Levine, B., Melia, T.J., Mizushima, N., Rubinsztein, D.C., Simonsen, A., et al., 2011. A comprehensive glossary of autophagy-related molecules and processes (2nd edition). Autophagy 7, 1273–1294.
Klionsky, D.J., Abdelmohsen, K., Abe, A., Abedin, M.J., Abeliovich, H., Acevedo Arozena, A., Adachi, H., Adams, C.M., Adams, P.D., Adeli, K., Adhihetty, P.J., Adler, S.G., Agam, G., Agarwal, R., Aghi, M.K., Agnello, M., Agostinis, P., Aguilar, P.V., Aguirre-Ghiso, J., Airoldi, E.M., et al., 2016. Guidelines for the use and interpretation of assays for monitoring autophagy (3rd edition). Autophagy 12, 1–222.
Levy, J.M.M., Towers, C.G., Thorburn, A., 2017. Targeting autophagy in cancer. Nat. Rev. Cancer 17, 528–542.
Li, X., Zhu, F., Jiang, J., Sun, C., Zhong, Q., Shen, M., Wang, X., Tian, R., Shi, C., Xu, M., Peng, F., Guo, X., Hu, J., Ye, D., Wang, M., Qin, R., 2016. Simultaneous inhibition of the ubiquitin-proteasome system and autophagy enhances apoptosis induced by ER stress aggravators in human pancreatic cancer cells. Autophagy 12, 1521–1537.
Medina, D.L., Fraldi, A., Bouche, V., Annunziata, F., Mansueto, G., Spampanato, C., Puri, C., Pignata, A., Martina, J.A., Sardiello, M., Palmieri, M., Polishchuk, R., Puertollano, R., Ballabio, A., 2011. Transcriptional activation of lysosomal exocytosis promotes

cellular clearance. Dev. Cell 21, 421–430.
Middleton, G., Palmer, D.H., Greenhalf, W., Ghaneh, P., Jackson, R., Cox, T., Evans, A., Shaw, V.E., Wadsley, J., Valle, J.W., Propper, D., Wasan, H., Falk, S., Cunningham, D., Coxon, F., Ross, P., Madhusudan, S., Wadd, N., Corrie, P., Hickish, T., et al., 2017. Vandetanib plus gemcitabine versus placebo plus gemcitabine in locally advanced or metastatic pancreatic carcinoma (ViP): a prospective, randomised, double-blind, multicentre phase 2 trial. Lancet Oncol. 18, 486–499.
Networ, T.C.G.A.R., 2017. Integrated genomic characterization of pancreatic ductal adenocarcinoma. Cancer Cell 32, 185–203 (e113).
Palmieri, M., Impey, S., Kang, H., di Ronza, A., Pelz, C., Sardiello, M., Ballabio, A., 2011. Characterization of the CLEAR network reveals an integrated control of cellular clearance pathways. Hum. Mol. Genet. 20, 3852–3866.
Rebecca, V.W., Amaravadi, R.K., 2016. Emerging strategies to effectively target autophagy in cancer. Oncogene 35, 1–11.
Rosenfeldt, M.T., O'Prey, J., Morton, J.P., Nixon, C., MacKay, G., Mrowinska, A., Au, A., Rai, T.S., Zheng, L., Ridgway, R., Adams, P.D., Anderson, K.I., Gottlieb, E., Sansom, O.J., Ryan, K.M., 2013. p53 status determines the role of autophagy in pancreatic tumour development. Nature 504, 296–300.
Rubinsztein, D.C., Marino, G., Kroemer, G., 2011. Autophagy and aging. Cell 146, 682–695.
Settembre, C., Ballabio, A., 2011. TFEB regulates autophagy: an integrated coordination of cellular degradation and recycling processes. Autophagy 7, 1379–1381.
Settembre, C., Di Malta, C., Polito, V.A., Garcia Arencibia, M., Vetrini, F., Erdin, S., Erdin, S.U., Huynh, T., Medina, D., Colella, P., Sardiello, M., Rubinsztein, D.C., Ballabio, A., 2011. TFEB links autophagy to lysosomal biogenesis. Science (New York, N.Y.) 332, 1429–1433.
Settembre, C., Fraldi, A., Medina, D.L., Ballabio, A., 2013. Signals from the lysosome: a control centre for cellular clearance and energy metabolism. Nat. Rev. Mol. Cell Biol. 14, 283–296.
Song, X.B., Liu, G., Liu, F., Yan, Z.G., Wang, Z.Y., Liu, Z.P., Wang, L., 2017. Autophagy blockade and lysosomal membrane permeabilization contribute to lead-induced nephrotoxicity in primary rat proximal tubular cells. Cell Death Dis. 8, e2863.
Tang, J.J., He, Q.R., Dong, S., Guo, X., Wang, Y.G., Lei, B.L., Tian, J.M., Gao, J.M., 2018. Diversity modification and structure-activity relationships of two natural products 1beta-hydroxy alantolactone and ivangustin as potent cytotoxic agents. Sci. Rep. 8, 1722.
TCGA, 2018. Pancreatic Cancer(PAAD) Dataset. UCSC Xena, USA. https://xenabrowser.net, Accessed date: 21 January 2018.
Torre, L.A., Bray, F., Siegel, R.L., Ferlay, J., Lortet-Tieulent, J., Jemal, A., 2015. Global cancer statistics, 2012. CA Cancer J. Clin. 65, 87–108.
Wang, X., Yu, Z., Wang, C., Cheng, W., Tian, X., Huo, X., Wang, Y., Sun, C., Feng, L., Xing, J., Lan, Y., Sun, D., Hou, Q., Zhang, B., Ma, X., Zhang, B., 2017. Alantolactone, a natural sesquiterpene lactone, has potent antitumor activity against glioblastoma by targeting IKKbeta kinase activity and interrupting NF-kappaB/COX-2-mediated signaling cascades. J. Exp. Clin. Cancer Res. 36, 93.
White, E., 2015. The role for autophagy in cancer. J. Clin. Invest. 125, 42–46.
Yang, A., Kimmelman, A.C., 2014. Inhibition of autophagy attenuates pancreatic cancer growth independent of TP53/TRP53 status. Autophagy 10, 1683–1684.
Yang, S., Wang, X., Contino, G., Liesa, M., Sahin, E., Ying, H., Bause, A., Li, Y., Stommel, J.M., Dell'antonio, G., Mautner, J., Tonon, G., Haigis, M., Shirihai, O.S., Doglioni, C., Bardeesy, N., Kimmelman, A.C., 2011. Pancreatic cancers require autophagy for tumor growth. Genes Dev. 25, 717–729.
Zhou, J., Tan, S.H., Nicolas, V., Bauvy, C., Yang, N.D., Zhang, J., Xue, Y., Codogno, P., Shen, H.M., 2013. Activation of lysosomal function in the course of autophagy via mTORC1 suppression and autophagosome-lysosome fusion. Cell Res. 23, 508–523.